

Measurement of the \bar{B}^0 Lifetime and of the $B^0\bar{B}^0$ Oscillation Frequency Using Partially Reconstructed $\bar{B}^0 \rightarrow D^{*+}\ell^-\bar{\nu}_\ell$ Decays

The BABAR Collaboration

December 9, 2018

Abstract

We present a simultaneous measurement of the \bar{B}^0 lifetime τ_{B^0} and mixing parameter Δm_d . We use a sample of about 50000 $\bar{B}^0 \rightarrow D^{*+}\ell^-\bar{\nu}_\ell$ partially reconstructed decays identified with the BABAR detector at the PEP-II storage ring at SLAC, where the flavor of the other B meson is determined from the charge of another high momentum lepton in the same event. The preliminary results are

$$\begin{aligned}\tau_{B^0} &= (1.501 \pm 0.008 \text{ (stat.)} \pm 0.030 \text{ (syst.)}) \text{ ps,} \\ \Delta m_d &= (0.523 \pm 0.004 \text{ (stat.)} \pm 0.007 \text{ (syst.)}) \text{ ps}^{-1}.\end{aligned}$$

Submitted to the 32nd International Conference on High-Energy Physics, ICHEP 04,
16 August—22 August 2004, Beijing, China

Stanford Linear Accelerator Center, Stanford University, Stanford, CA 94309

Work supported in part by Department of Energy contract DE-AC03-76SF00515.

The BABAR Collaboration,

B. Aubert, R. Barate, D. Boutigny, F. Couderc, J.-M. Gaillard, A. Hicheur, Y. Karyotakis, J. P. Lees,
V. Tisserand, A. Zghiche

Laboratoire de Physique des Particules, F-74941 Annecy-le-Vieux, France

A. Palano, A. Pompili

Università di Bari, Dipartimento di Fisica and INFN, I-70126 Bari, Italy

J. C. Chen, N. D. Qi, G. Rong, P. Wang, Y. S. Zhu

Institute of High Energy Physics, Beijing 100039, China

G. Eigen, I. Ofte, B. Stugu

University of Bergen, Inst. of Physics, N-5007 Bergen, Norway

G. S. Abrams, A. W. Borgland, A. B. Breon, D. N. Brown, J. Button-Shafer, R. N. Cahn, E. Charles,
C. T. Day, M. S. Gill, A. V. Gritsan, Y. Groysman, R. G. Jacobsen, R. W. Kadel, J. Kadyk, L. T. Kerth,
Yu. G. Kolomensky, G. Kukartsev, G. Lynch, L. M. Mir, P. J. Oddone, T. J. Orimoto, M. Pripstein,
N. A. Roe, M. T. Ronan, V. G. Shelkov, W. A. Wenzel

Lawrence Berkeley National Laboratory and University of California, Berkeley, CA 94720, USA

M. Barrett, K. E. Ford, T. J. Harrison, A. J. Hart, C. M. Hawkes, S. E. Morgan, A. T. Watson

University of Birmingham, Birmingham, B15 2TT, United Kingdom

M. Fritsch, K. Goetzen, T. Held, H. Koch, B. Lewandowski, M. Pelizaeus, M. Steinke
Ruhr Universität Bochum, Institut für Experimentalphysik 1, D-44780 Bochum, Germany

J. T. Boyd, N. Chevalier, W. N. Cottingham, M. P. Kelly, T. E. Latham, F. F. Wilson

University of Bristol, Bristol BS8 1TL, United Kingdom

T. Cuhadar-Donszelmann, C. Hearty, N. S. Knecht, T. S. Mattison, J. A. McKenna, D. Thiessen

University of British Columbia, Vancouver, BC, Canada V6T 1Z1

A. Khan, P. Kyberd, L. Teodorescu

Brunel University, Uxbridge, Middlesex UB8 3PH, United Kingdom

A. E. Blinov, V. E. Blinov, V. P. Druzhinin, V. B. Golubev, V. N. Ivanchenko, E. A. Kravchenko,
A. P. Onuchin, S. I. Serebnyakov, Yu. I. Skovpen, E. P. Solodov, A. N. Yushkov

Budker Institute of Nuclear Physics, Novosibirsk 630090, Russia

D. Best, M. Bruinsma, M. Chao, I. Eschrich, D. Kirkby, A. J. Lankford, M. Mandelkern, R. K. Mommsen,
W. Roethel, D. P. Stoker

University of California at Irvine, Irvine, CA 92697, USA

C. Buchanan, B. L. Hartfiel

University of California at Los Angeles, Los Angeles, CA 90024, USA

S. D. Foulkes, J. W. Gary, B. C. Shen, K. Wang

University of California at Riverside, Riverside, CA 92521, USA

- D. del Re, H. K. Hadavand, E. J. Hill, D. B. MacFarlane, H. P. Paar, Sh. Rahatlou, V. Sharma
University of California at San Diego, La Jolla, CA 92093, USA
- J. W. Berryhill, C. Campagnari, B. Dahmes, O. Long, A. Lu, M. A. Mazur, J. D. Richman, W. Verkerke
University of California at Santa Barbara, Santa Barbara, CA 93106, USA
- T. W. Beck, A. M. Eisner, C. A. Heusch, J. Kroseberg, W. S. Lockman, G. Nesom, T. Schalk,
B. A. Schumm, A. Seiden, P. Spradlin, D. C. Williams, M. G. Wilson
University of California at Santa Cruz, Institute for Particle Physics, Santa Cruz, CA 95064, USA
- J. Albert, E. Chen, G. P. Dubois-Felsmann, A. Dvoretzkii, D. G. Hitlin, I. Narsky, T. Piatenko,
F. C. Porter, A. Ryd, A. Samuel, S. Yang
California Institute of Technology, Pasadena, CA 91125, USA
- S. Jayatileke, G. Mancinelli, B. T. Meadows, M. D. Sokoloff
University of Cincinnati, Cincinnati, OH 45221, USA
- T. Abe, F. Blanc, P. Bloom, S. Chen, W. T. Ford, U. Nauenberg, A. Olivas, P. Rankin, J. G. Smith,
J. Zhang, L. Zhang
University of Colorado, Boulder, CO 80309, USA
- A. Chen, J. L. Harton, A. Soffer, W. H. Toki, R. J. Wilson, Q. Zeng
Colorado State University, Fort Collins, CO 80523, USA
- D. Altenburg, T. Brandt, J. Brose, M. Dickopp, E. Feltresi, A. Hauke, H. M. Lacker, R. Müller-Pfefferkorn,
R. Nogowski, S. Otto, A. Petzold, J. Schubert, K. R. Schubert, R. Schwierz, B. Spaan, J. E. Sundermann
Technische Universität Dresden, Institut für Kern- und Teilchenphysik, D-01062 Dresden, Germany
- D. Bernard, G. R. Bonneaud, F. Brochard, P. Grenier, S. Schrenk, Ch. Thiebaux, G. Vasileiadis, M. Verderi
Ecole Polytechnique, LLR, F-91128 Palaiseau, France
- D. J. Bard, P. J. Clark, D. Lavin, F. Muheim, S. Playfer, Y. Xie
University of Edinburgh, Edinburgh EH9 3JZ, United Kingdom
- M. Andreotti, V. Azzolini, D. Bettoni, C. Bozzi, R. Calabrese, G. Cibinetto, E. Luppi, M. Negrini,
L. Piemontese, A. Sarti
Università di Ferrara, Dipartimento di Fisica and INFN, I-44100 Ferrara, Italy
- E. Treadwell
Florida A&M University, Tallahassee, FL 32307, USA
- F. Anulli, R. Baldini-Ferroli, A. Calcaterra, R. de Sangro, G. Finocchiaro, P. Patteri, I. M. Peruzzi,
M. Piccolo, A. Zallo
Laboratori Nazionali di Frascati dell'INFN, I-00044 Frascati, Italy
- A. Buzzo, R. Capra, R. Contri, G. Crosetti, M. Lo Vetere, M. Macri, M. R. Monge, S. Passaggio,
C. Patrignani, E. Robutti, A. Santroni, S. Tosi
Università di Genova, Dipartimento di Fisica and INFN, I-16146 Genova, Italy
- S. Bailey, G. Brandenburg, K. S. Chaisanguanthum, M. Morii, E. Won
Harvard University, Cambridge, MA 02138, USA

R. S. Dubitzky, U. Langenegger

Universität Heidelberg, Physikalisches Institut, Philosophenweg 12, D-69120 Heidelberg, Germany

W. Bhimji, D. A. Bowerman, P. D. Dauncey, U. Egede, J. R. Gaillard, G. W. Morton, J. A. Nash,
M. B. Nikolich, G. P. Taylor

Imperial College London, London, SW7 2AZ, United Kingdom

M. J. Charles, G. J. Grenier, U. Mallik

University of Iowa, Iowa City, IA 52242, USA

J. Cochran, H. B. Crawley, J. Lamsa, W. T. Meyer, S. Prell, E. I. Rosenberg, A. E. Rubin, J. Yi

Iowa State University, Ames, IA 50011-3160, USA

M. Biasini, R. Covarelli, M. Pioppi

Università di Perugia, Dipartimento di Fisica and INFN, I-06100 Perugia, Italy

M. Davier, X. Giroux, G. Grosdidier, A. Höcker, S. Laplace, F. Le Diberder, V. Lepeltier, A. M. Lutz,
T. C. Petersen, S. Plaszczynski, M. H. Schune, L. Tantot, G. Wormser

Laboratoire de l'Accélérateur Linéaire, F-91898 Orsay, France

C. H. Cheng, D. J. Lange, M. C. Simani, D. M. Wright

Lawrence Livermore National Laboratory, Livermore, CA 94550, USA

A. J. Bevan, C. A. Chavez, J. P. Coleman, I. J. Forster, J. R. Fry, E. Gabathuler, R. Gamet,
D. E. Hutchcroft, R. J. Parry, D. J. Payne, R. J. Sloane, C. Touramanis

University of Liverpool, Liverpool L69 7ZE, United Kingdom

J. J. Back,¹ C. M. Cormack, P. F. Harrison,¹ F. Di Lodovico, G. B. Mohanty¹

Queen Mary, University of London, E1 4NS, United Kingdom

C. L. Brown, G. Cowan, R. L. Flack, H. U. Flaecher, M. G. Green, P. S. Jackson, T. R. McMahon,
S. Ricciardi, F. Salvatore, M. A. Winter

*University of London, Royal Holloway and Bedford New College, Egham, Surrey TW20 0EX,
United Kingdom*

D. Brown, C. L. Davis

University of Louisville, Louisville, KY 40292, USA

J. Allison, N. R. Barlow, R. J. Barlow, P. A. Hart, M. C. Hodgkinson, G. D. Lafferty, A. J. Lyon,
J. C. Williams

University of Manchester, Manchester M13 9PL, United Kingdom

A. Farbin, W. D. Hulsbergen, A. Jawahery, D. Kovalskyi, C. K. Lae, V. Lillard, D. A. Roberts

University of Maryland, College Park, MD 20742, USA

G. Blaylock, C. Dallapiccola, K. T. Flood, S. S. Hertzbach, R. Kofler, V. B. Koptchev, T. B. Moore,
S. Saremi, H. Staengle, S. Willocq

University of Massachusetts, Amherst, MA 01003, USA

¹Now at Department of Physics, University of Warwick, Coventry, United Kingdom

R. Cowan, G. Sciolla, S. J. Sekula, F. Taylor, R. K. Yamamoto
Massachusetts Institute of Technology, Laboratory for Nuclear Science, Cambridge, MA 02139, USA

D. J. J. Mangeol, P. M. Patel, S. H. Robertson
McGill University, Montréal, QC, Canada H3A 2T8

A. Lazzaro, V. Lombardo, F. Palombo
Università di Milano, Dipartimento di Fisica and INFN, I-20133 Milano, Italy

J. M. Bauer, L. Cremaldi, V. Eschenburg, R. Godang, R. Kroeger, J. Reidy, D. A. Sanders, D. J. Summers,
H. W. Zhao
University of Mississippi, University, MS 38677, USA

S. Brunet, D. Côté, P. Taras
Université de Montréal, Laboratoire René J. A. Lévesque, Montréal, QC, Canada H3C 3J7

H. Nicholson
Mount Holyoke College, South Hadley, MA 01075, USA

N. Cavallo,² F. Fabozzi,² C. Gatto, L. Lista, D. Monorchio, P. Paolucci, D. Piccolo, C. Sciacca
Università di Napoli Federico II, Dipartimento di Scienze Fisiche and INFN, I-80126, Napoli, Italy

M. Baak, H. Bulten, G. Raven, H. L. Snoek, L. Wilden
*NIKHEF, National Institute for Nuclear Physics and High Energy Physics, NL-1009 DB Amsterdam,
The Netherlands*

C. P. Jessop, J. M. LoSecco
University of Notre Dame, Notre Dame, IN 46556, USA

T. Allmendinger, K. K. Gan, K. Honscheid, D. Hufnagel, H. Kagan, R. Kass, T. Pulliam, A. M. Rahimi,
R. Ter-Antonyan, Q. K. Wong
Ohio State University, Columbus, OH 43210, USA

J. Brau, R. Frey, O. Igonkina, C. T. Potter, N. B. Sinev, D. Strom, E. Torrence
University of Oregon, Eugene, OR 97403, USA

F. Colecchia, A. Dorigo, F. Galeazzi, M. Margoni, M. Morandin, M. Posocco, M. Rotondo, F. Simonetto,
R. Stroili, G. Tiozzo, C. Voci
Università di Padova, Dipartimento di Fisica and INFN, I-35131 Padova, Italy

M. Benayoun, H. Briand, J. Chauveau, P. David, Ch. de la Vaissière, L. Del Buono, O. Hamon,
M. J. J. John, Ph. Leruste, J. Malcles, J. Ocariz, M. Pivk, L. Roos, S. T'Jampens, G. Therin
*Universités Paris VI et VII, Laboratoire de Physique Nucléaire et de Hautes Energies, F-75252 Paris,
France*

P. F. Manfredi, V. Re
Università di Pavia, Dipartimento di Elettronica and INFN, I-27100 Pavia, Italy

²Also with Università della Basilicata, Potenza, Italy

P. K. Behera, L. Gladney, Q. H. Guo, J. Panetta
University of Pennsylvania, Philadelphia, PA 19104, USA

C. Angelini, G. Batignani, S. Bettarini, M. Bondioli, F. Bucci, G. Calderini, M. Carpinelli, F. Forti,
M. A. Giorgi, A. Lusiani, G. Marchiori, F. Martinez-Vidal,³ M. Morganti, N. Neri, E. Paoloni, M. Rama,
G. Rizzo, F. Sandrelli, J. Walsh
Università di Pisa, Dipartimento di Fisica, Scuola Normale Superiore and INFN, I-56127 Pisa, Italy

M. Haire, D. Judd, K. Paick, D. E. Wagoner
Prairie View A&M University, Prairie View, TX 77446, USA

N. Danielson, P. Elmer, Y. P. Lau, C. Lu, V. Miftakov, J. Olsen, A. J. S. Smith, A. V. Telnov
Princeton University, Princeton, NJ 08544, USA

F. Bellini, G. Cavoto,⁴ R. Faccini, F. Ferrarotto, F. Ferroni, M. Gaspero, L. Li Gioi, M. A. Mazzoni,
S. Morganti, M. Pierini, G. Piredda, F. Safai Tehrani, C. Voena
Università di Roma La Sapienza, Dipartimento di Fisica and INFN, I-00185 Roma, Italy

S. Christ, G. Wagner, R. Waldi
Universität Rostock, D-18051 Rostock, Germany

T. Adye, N. De Groot, B. Franek, N. I. Geddes, G. P. Gopal, E. O. Olaiya
Rutherford Appleton Laboratory, Chilton, Didcot, Oxon, OX11 0QX, United Kingdom

R. Aleksan, S. Emery, A. Gaidot, S. F. Ganzhur, P.-F. Giraud, G. Hamel de Monchenault, W. Kozanecki,
M. Legendre, G. W. London, B. Mayer, G. Schott, G. Vasseur, Ch. Yèche, M. Zito
DSM/Daphnia, CEA/Saclay, F-91191 Gif-sur-Yvette, France

M. V. Purohit, A. W. Weidemann, J. R. Wilson, F. X. Yumiceva
University of South Carolina, Columbia, SC 29208, USA

D. Aston, R. Bartoldus, N. Berger, A. M. Boyarski, O. L. Buchmueller, R. Claus, M. R. Convery,
M. Cristinziani, G. De Nardo, D. Dong, J. Dorfan, D. Dujmic, W. Dunwoodie, E. E. Elsen, S. Fan,
R. C. Field, T. Glanzman, S. J. Gowdy, T. Hadig, V. Halyo, C. Hast, T. Hryn'ova, W. R. Innes,
M. H. Kelsey, P. Kim, M. L. Kocian, D. W. G. S. Leith, J. Libby, S. Luitz, V. Luth, H. L. Lynch,
H. Marsiske, R. Messner, D. R. Muller, C. P. O'Grady, V. E. Ozcan, A. Perazzo, M. Perl, S. Petrak,
B. N. Ratcliff, A. Roodman, A. A. Salnikov, R. H. Schindler, J. Schwiening, G. Simi, A. Snyder, A. Soha,
J. Stelzer, D. Su, M. K. Sullivan, J. Va'vra, S. R. Wagner, M. Weaver, A. J. R. Weinstein,
W. J. Wisniewski, M. Wittgen, D. H. Wright, A. K. Yarritu, C. C. Young
Stanford Linear Accelerator Center, Stanford, CA 94309, USA

P. R. Burchat, A. J. Edwards, T. I. Meyer, B. A. Petersen, C. Roat
Stanford University, Stanford, CA 94305-4060, USA

S. Ahmed, M. S. Alam, J. A. Ernst, M. A. Saeed, M. Saleem, F. R. Wappler
State University of New York, Albany, NY 12222, USA

³Also with IFIC, Instituto de Física Corpuscular, CSIC-Universidad de Valencia, Valencia, Spain

⁴Also with Princeton University, Princeton, USA

W. Bugg, M. Krishnamurthy, S. M. Spanier
University of Tennessee, Knoxville, TN 37996, USA

R. Eckmann, H. Kim, J. L. Ritchie, A. Satpathy, R. F. Schwitters
University of Texas at Austin, Austin, TX 78712, USA

J. M. Izen, I. Kitayama, X. C. Lou, S. Ye
University of Texas at Dallas, Richardson, TX 75083, USA

F. Bianchi, M. Bona, F. Gallo, D. Gamba
Università di Torino, Dipartimento di Fisica Sperimentale and INFN, I-10125 Torino, Italy

L. Bosisio, C. Cartaro, F. Cossutti, G. Della Ricca, S. Dittongo, S. Grancagnolo, L. Lanceri, P. Poropat,⁵
L. Vitale, G. Vuagnin
Università di Trieste, Dipartimento di Fisica and INFN, I-34127 Trieste, Italy

R. S. Panvini
Vanderbilt University, Nashville, TN 37235, USA

Sw. Banerjee, C. M. Brown, D. Fortin, P. D. Jackson, R. Kowalewski, J. M. Roney, R. J. Sobie
University of Victoria, Victoria, BC, Canada V8W 3P6

H. R. Band, B. Cheng, S. Dasu, M. Datta, A. M. Eichenbaum, M. Graham, J. J. Hollar, J. R. Johnson,
P. E. Kutter, H. Li, R. Liu, A. Mihalyi, A. K. Mohapatra, Y. Pan, R. Prepost, P. Tan, J. H. von
Wimmersperg-Toeller, J. Wu, S. L. Wu, Z. Yu
University of Wisconsin, Madison, WI 53706, USA

M. G. Greene, H. Neal
Yale University, New Haven, CT 06511, USA

⁵Deceased

1 INTRODUCTION

The time evolution of \bar{B}^0 mesons is governed by the overall decay rate $\Gamma(\bar{B}^0) = 1/\tau_{B^0}$ and by the mass difference Δm_d of the two mass eigenstates. A precise determination of $\Gamma(\bar{B}^0)$ reduces the systematic error on the parameters $|V_{cb}|$ and $|V_{ub}|$ of the Cabibbo-Kobayashi-Maskawa flavor mixing matrix. The parameter $|V_{td}V_{tb}^*|$ enters the box diagram that is responsible for $B^0\bar{B}^0$ oscillations and can be determined from a measurement of Δm_d , with a sizeable systematic error due to theoretical uncertainties.

We describe here a measurement of τ_{B^0} and Δm_d performed using $\bar{B}^0 \rightarrow D^{*+}\ell^-\bar{\nu}_\ell$ decays⁶ selected from a sample of about 88 million $B\bar{B}$ events recorded by the *BABAR* detector at the PEP-II asymmetric-energy e^+e^- storage ring, operated at or near the $\Upsilon(4S)$ resonance. $B\bar{B}$ pairs from the $\Upsilon(4S)$ decay move along the beam axis with a nominal Lorentz boost $\langle\beta\gamma\rangle = 0.55$, so that the vertices from the two B -decay points are separated on average by about 260 μm . The $B^0\bar{B}^0$ system is produced in a coherent P -wave state, so that flavor oscillation is measurable only relative to the decay of the first B meson. Mixed (unmixed) events are selected by the observation of two equal (opposite) flavor B meson decays. The probabilities of observing mixed (\mathcal{S}^-) or unmixed (\mathcal{S}^+) events as a function of the proper time difference Δt are

$$\mathcal{S}^\pm = \frac{e^{-|\Delta t|/\tau_{B^0}}}{4\tau_{B^0}}(1 \pm \mathcal{D} \cos(\Delta m_d \Delta t)), \quad (1)$$

where \mathcal{D} is related to the fraction w of events with wrong flavor assignment by the relation $\mathcal{D} = 1 - 2w$ and Δt is computed from the distance between the two vertices projected along the beam direction.

2 THE *BABAR* DETECTOR AND DATASET

We have analyzed a data sample of 81 fb^{-1} collected by *BABAR* on the $\Upsilon(4S)$ resonance, a sample of 9.6 fb^{-1} below the resonance, to study the continuum background, and a sample of $B\bar{B}$ simulated events corresponding to about three times the size of the data sample. The simulated events are processed through the same analysis chain as the real data. *BABAR* is a multi-purpose detector, described in detail in Ref. [1]. The momentum of charged particles is measured by the tracking system, which consists of a silicon vertex tracker (SVT) and a drift chamber (DCH) in a 1.5-T magnetic field. The SVT measures the momentum of low transverse momentum charged tracks that do not reach the DCH due to bending in the magnetic field. The energy loss in the SVT is used in this analysis to discriminate low-momentum pions from electrons. Higher-energy electrons are identified from the ratio of the energy of their associated shower in the electromagnetic calorimeter (EMC) to their momentum, the transverse profile of the shower, the energy loss in the DCH, and the information from the Cherenkov detector (DIRC). The electron identification efficiency within the tracking volume is about 90%, and the hadron misidentification probability is less than 1%. Muons are identified on the basis of the energy deposit in the EMC and the penetration in the instrumented flux return. Muon candidates compatible with the kaon hypothesis in the DIRC are rejected. The muon identification efficiency is about 60%, and the hadron misidentification rate is about 2%.

⁶Charge conjugate states are always implicitly assumed; ℓ means either electron or muon.

3 ANALYSIS METHOD

3.1 Selection of $\bar{B}^0 \rightarrow D^{*+} \ell^- \bar{\nu}_\ell$ decays

We select events that have more than four charged tracks. We reduce the contamination from light-quark production in continuum events by requiring the normalized Fox-Wolfram second moment [2] to be less than 0.5. We select $\bar{B}^0 \rightarrow D^{*+} \ell^- \bar{\nu}_\ell$ events with partial reconstruction of the decay $D^{*+} \rightarrow \pi_s^+ D^0$, using only the charged lepton and the soft pion (π_s^+) from the D^{*+} . The D^0 is not reconstructed, resulting in high reconstruction efficiency. *BABAR* has already published two measurements of τ_{B^0} [3, 4] and a measurement of $\sin(2\beta + \gamma)$ [5] based on partial reconstruction. This technique was originally applied to $\bar{B}^0 \rightarrow D^{*+} \ell^- \bar{\nu}_\ell$ decays by ARGUS [6], and then used by CLEO [7], DELPHI [8], and OPAL [9]. This is, however, the first simultaneous measurement of τ_{B^0} and Δm_d based on partial reconstruction.

To suppress leptons from several background sources, we use only high momentum leptons, in the range $1.3 < p < 2.4$ GeV/ c .⁷ The π_s^+ candidates have momenta between 60 and 200 MeV/ c . Due to the limited phase space available in the D^{*+} decay, the π_s^+ is emitted within approximately a one-radian full opening angle cone centered about the D^{*+} flight direction (in the $\Upsilon(4S)$ frame). Therefore, we approximate the direction of the D^{*+} to be that of the π_s^+ and estimate the energy $\tilde{E}_{D^{*+}}$ of the D^{*+} as a function of the energy of the π_s^+ using a third order polynomial, with parameters taken from the simulation. We define the square of the missing neutrino mass as

$$\mathcal{M}_\nu^2 = \left(\frac{\sqrt{s}}{2} - \tilde{E}_{D^{*+}} - E_\ell\right)^2 - (\tilde{\mathbf{p}}_{D^{*+}} + \mathbf{p}_\ell)^2,$$

where we neglect the momentum of the \bar{B}^0 in the $\Upsilon(4S)$ frame (on average, 0.34 GeV/ c), and identify its energy with the beam energy $\sqrt{s}/2$ in the e^+e^- center-of-mass frame. E_ℓ and \mathbf{p}_ℓ are the energy and momentum vector of the lepton and $\tilde{\mathbf{p}}_{D^{*+}}$ is the estimated momentum vector of the D^{*+} . The distribution of \mathcal{M}_ν^2 peaks at zero for signal events, while it is spread over a wide range for background events (see Fig. 1).

We determine the \bar{B}^0 decay point from a vertex fit of the ℓ and π_s^+ tracks, constrained to the beam spot position in the plane perpendicular to the beam axis (the $x - y$ plane). The beam spot position and size are determined on a run-by-run basis using two-prong events [1]. Its size in the horizontal (x) direction is 120 μm . Although the beam spot size in the vertical (y) direction is only 5.6 μm , we use a constraint of 50 μm in the vertex fit to account for the flight distance of the \bar{B}^0 in the $x - y$ plane. We reject events for which the χ^2 probability of the vertex fit, \mathcal{P}_V , does not exceed 0.1%.

We then apply a selection criterion to a combined signal likelihood, calculated from p_ℓ , $p_{\pi_s^+}$, and \mathcal{P}_V , which results in a signal-to-background ratio of about one-to-one in the signal region defined as $\mathcal{M}_\nu^2 > -2.5$ GeV²/ c^4 . Figure 1 shows the distribution of \mathcal{M}_ν^2 for the events selected at this stage of the analysis. The plot on the top is obtained from the events in which the ℓ and the π_s have opposite charges (“right-charge”), the plot at the bottom from events where ℓ and the π_s have equal charges (“wrong-charge”). We use wrong-charge events as a background control sample, to verify that the $B\bar{B}$ combinatorial background is described well by the simulation. To do this, we add the off-peak events, scaled by the ratio of the on-peak to the off-peak luminosities, to the $B\bar{B}$ Monte Carlo scaled to match the data in the region $\mathcal{M}_\nu^2 < -4.5$ GeV²/ c^4 . We then compare the expected

⁷The lepton and pion momenta, the π_s^+ direction, and $\tilde{E}_{D^{*+}}$ (see below) are always computed in the $\Upsilon(4S)$ rest frame.

number of events to the number of data events in the signal region. This ratio is 0.996 ± 0.002 , consistent with unity. For the rest of the analysis we only consider right-charge events.

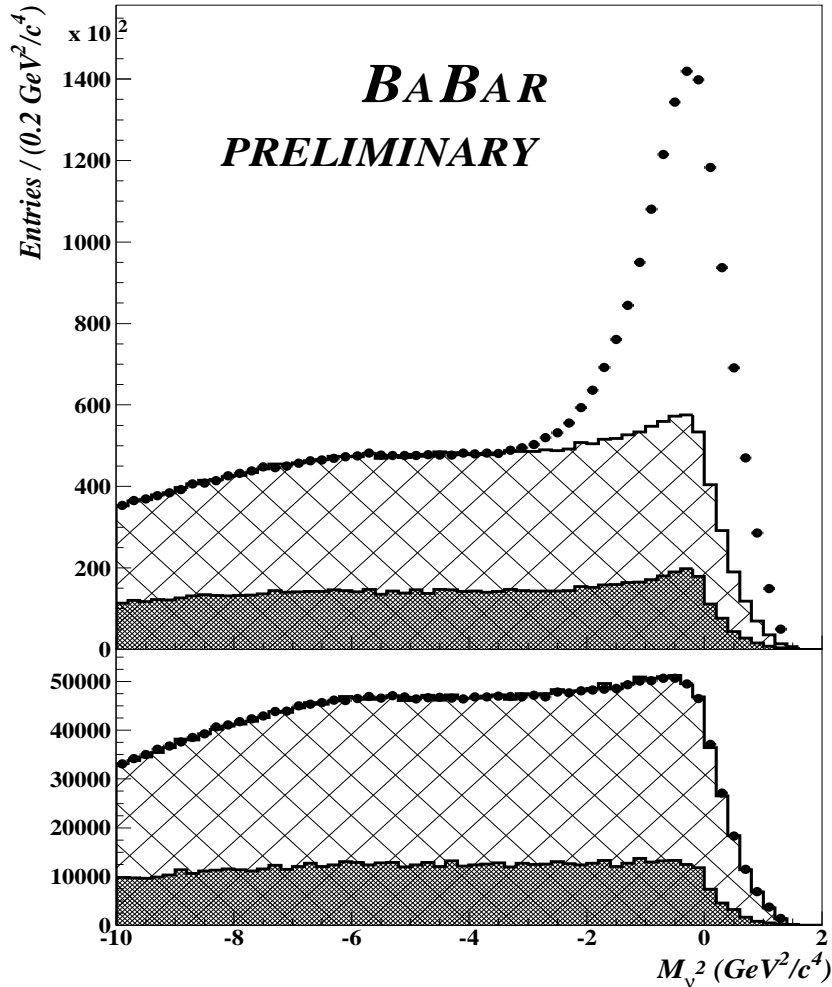


Figure 1: M_V^2 distribution for the right-charge (top) and wrong-charge (bottom) events. The points correspond to on resonance data. The distributions of continuum events (dark histogram), obtained from rescaled off-peak events, and $B\bar{B}$ combinatorial events (hatched area), obtained from the simulation, are overlaid.

3.2 Tag Vertex and B Flavor Tagging

We restrict the analysis to events in which another charged lepton (“tagging lepton”) is found. To reduce contamination from fake leptons and leptons originating from charm decays, we require that the momentum of the lepton exceeds $1.0 \text{ GeV}/c$ for electrons, $1.1 \text{ GeV}/c$ for muons. The tagging lepton is used to tag the flavor of the other (“tag”) B . The decay point of the tag B is computed from the intersection of the tagging lepton track with a beam-spot ellipse centered on the position

of the reconstructed B . The beam spot constraint is applied only in the transverse plane, and the width in the vertical direction is inflated to $50\mu\text{m}$. We compute the proper time difference Δt between the two vertices from their projected distance along the beam direction (z -axis), Δz , neglecting the \bar{B}^0 motion in the $\Upsilon(4S)$ rest frame (boost approximation). We obtain $\Delta t = \frac{\Delta z}{c\beta\gamma}$, where the boost factor $\beta\gamma$ is determined from the continuously measured beam energies. To remove badly reconstructed vertices we reject all events with either $|\Delta z| > 3\text{ mm}$ or $\sigma(\Delta z) > 0.5\text{ mm}$, where $\sigma(\Delta z)$ is the uncertainty on Δz , computed for each event. The simulation shows that the rms of the difference between the true and measured Δt is 0.64 ps for 70% of the events, and about 1.7 ps for the rest. We then select only one right-charge candidate per event according to the following procedure: if there is more than one candidate in the event, we choose the one lying in the region $\mathcal{M}_\nu^2 > -2.5\text{ GeV}^2/c^4$. We reject the event if there is more than one candidate (either right or wrong charge) in this region. This criterion reduces by about 20% the number of signal events. For background studies, we select events in the region $\mathcal{M}_\nu^2 < -2.5\text{ GeV}^2/c^4$ if there is no candidate in the region $\mathcal{M}_\nu^2 > -2.5\text{ GeV}^2/c^4$. We find about 50000 signal events over a background of about 27000 events in the data sample.

3.3 Sample Composition

Our data sample consists of the following event types, categorized according to their origin and to whether or not they exhibit a peak in the \mathcal{M}_ν^2 distribution. We consider signal to be any combination of a lepton and a charged D^* produced in the decay of the same \bar{B}^0 meson. Signal consists mainly of $\bar{B}^0 \rightarrow D^{*+}\ell^-\bar{\nu}_\ell$ decays, with minor contributions from $\bar{B}^0 \rightarrow D^{*+}\pi^0\ell^-\bar{\nu}_\ell$, $\bar{B}^0 \rightarrow D^{*+}\tau^-\bar{\nu}_\tau$, $\bar{B}^0 \rightarrow D^{*+}D_s^-$, $\bar{B}^0 \rightarrow D^{*+}\bar{D}X$ with τ , D_s^- , or \bar{D} decaying to an ℓ^- , and $\bar{B}^0 \rightarrow D^{*+}h$, with the hadron h misidentified as a muon. A peaking B^- background is due to the process $B^- \rightarrow D^{*+}\pi^-\ell^-\bar{\nu}_\ell$. Non-peaking contributions are due to random combinations of a charged lepton candidate and a low-momentum pion candidate, produced either in $B\bar{B}$ events ($B\bar{B}$ combinatorial) or in $e^+e^- \rightarrow q\bar{q}$ interactions with $q = u, d, s$ or c (continuum). We compute the sample composition separately for mixed and unmixed events by fitting the corresponding \mathcal{M}_ν^2 distribution to the sum of four components: continuum, $B\bar{B}$ combinatorial, $\bar{B}^0 \rightarrow D^{*+}\ell^-\bar{\nu}_\ell$ decays, and $B \rightarrow D^*\pi\ell^-\bar{\nu}_\ell$ decays. Due to the production of one or more additional pions, these latter events have a different \mathcal{M}_ν^2 spectrum from that of the direct process $\bar{B}^0 \rightarrow D^{*+}\ell^-\bar{\nu}_\ell$. We measure the continuum contribution from the off-resonance sample, scaled to the luminosity of the on-resonance sample. We determine the \mathcal{M}_ν^2 distributions for the other event types from the simulation, and determine their relative abundance in the selected sample from a fit to the \mathcal{M}_ν^2 distribution for the data. Assuming isospin conservation, we assign two thirds of $B \rightarrow D^*\pi\ell^-\bar{\nu}_\ell$ decays to peaking B^- background and the rest to $\bar{B}^0 \rightarrow D^*\pi\ell^-\bar{\nu}_\ell$, which we add to the signal. We vary this fraction in the study of systematic uncertainties. We assume 50% error on the isospin hypothesis that allows us to determine the peaking B^- contribution.

A possible bias in the \mathcal{M}_ν^2 distribution comes from the decay chain $\bar{B} \rightarrow \ell^-\bar{\nu}_\ell D(X)$, $D \rightarrow Y\pi^+$, where the state Y is so heavy that the charged pion is emitted at low momentum, behaving like a π_s^+ . This possibility has been extensively studied by the CLEO collaboration in Ref. [10], where the three D^+ decay modes most likely to cause this bias have been identified: $\bar{K}^{*0}\omega\pi^+$, $K^{*-}\rho^+\pi^+$ and $\bar{K}^{*0}\rho^0\pi^+$. They quote a systematic error of $\pm 2.3\%$ on the background rate as a result of that analysis. Based on their result, we attribute the same systematic error to the number of combinatorial events below the signal mass peak.

Figure 2 shows the fit results for unmixed (left) and mixed (right) events. We use the results

of this study to determine the fraction of continuum (f_{qq}^\pm), $B\bar{B}$ combinatorial ($f_{B\bar{B}}^\pm$), and peaking B^- background ($f_{B^-}^\pm$) as a function of M_ν^2 , separately for mixed (f^-) and unmixed (f^+) events. We parameterize these fractions with polynomial functions, as shown in Fig. 3.

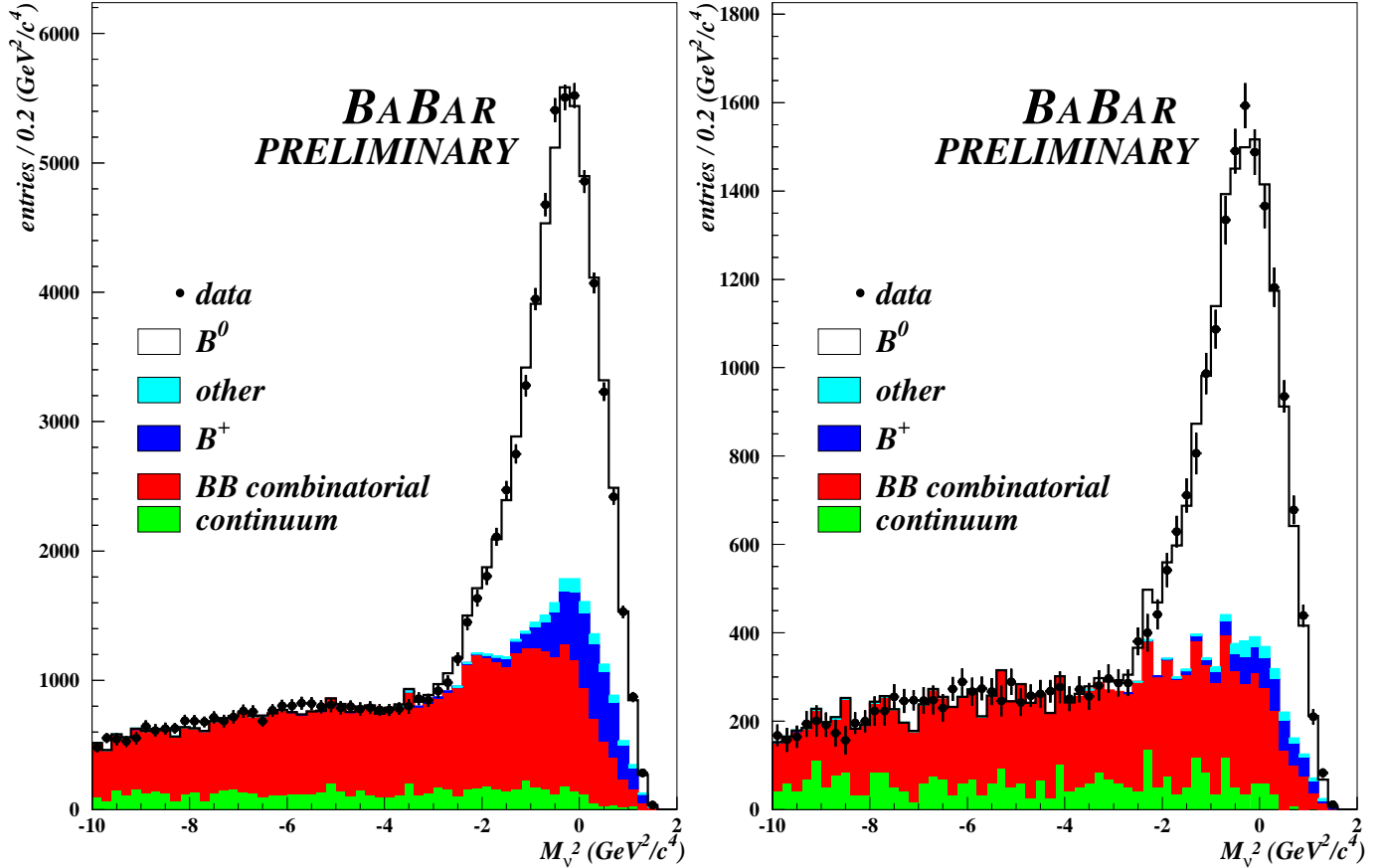


Figure 2: Fit to the M_ν^2 distribution for the unmixed events (left) and mixed events (right). “ B^0 ” includes $\bar{B}^0 \rightarrow D^{*+}\ell^-\bar{\nu}_\ell$, $\bar{B}^0 \rightarrow D^{*+}\pi^0\ell\nu_\ell$, $\bar{B}^0 \rightarrow D^{*+}\nu_\tau\tau^-$ ($\tau \rightarrow \ell$), $\bar{B}^0 \rightarrow D^{*+}D_s^-$ ($D_s \rightarrow \ell$), and $\bar{B}^0 \rightarrow D^{*+}h$ with the hadron h misidentified as a muon. “ B^+ ” includes $B^+ \rightarrow D^{*-}\pi^+\ell\nu_\ell$ and $B^+ \rightarrow D^{*-}\pi^+X$ with the π^+ misidentified as a muon. “Other” includes $B \rightarrow D^*\pi\nu_\tau\tau$ ($\tau \rightarrow \ell$), $B \rightarrow D^*\bar{D}X$ ($\bar{D} \rightarrow \ell Y$), and $B \rightarrow D^*\pi h$ with the hadron h misidentified as a muon.

3.4 τ_{B^0} and Δm_d Determination

We fit data and Monte Carlo events with a binned maximum-likelihood method. We divide our events into one hundred Δt bins, spanning the range $-18 \text{ ps} < \Delta t < 18 \text{ ps}$, and twenty $\sigma_{\Delta t}$ bins between 0 and 3 ps. We assign to all events in each bin the values of Δt and $\sigma_{\Delta t}$ corresponding to the center of the bin. We fit simultaneously the mixed and unmixed events. We do not use an extended likelihood, but instead apply a constraint on the fraction of mixed events, which, for a

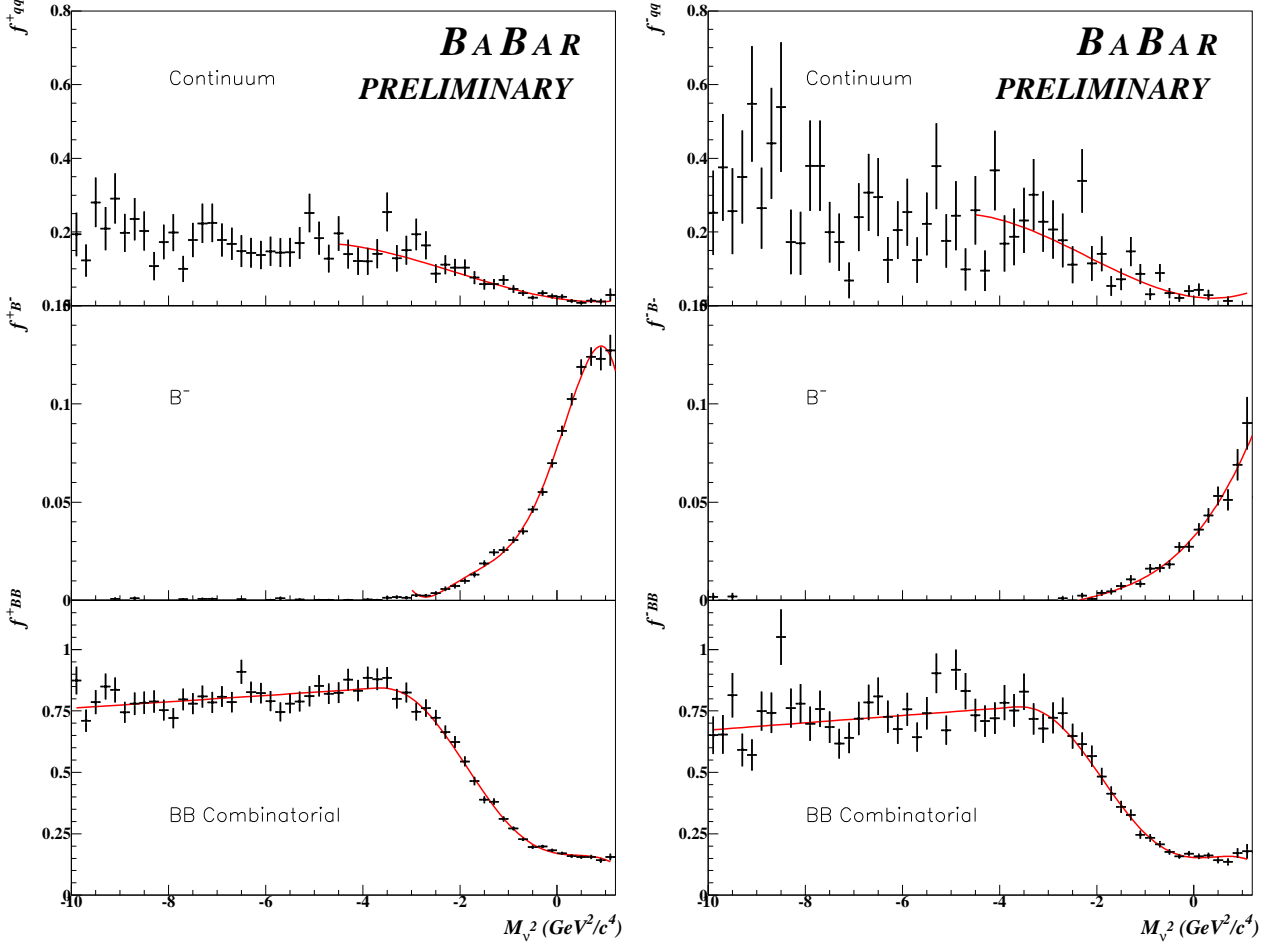


Figure 3: Fraction of continuum events, peaking B^- , and $B\bar{B}$ combinatorial background in the unmixed (left) and mixed (right) lepton-tagged samples. The fraction of continuum events, f_{qq}^{\pm} , is parameterized only in the region $\mathcal{M}_{\nu}^2 > -4.5 \text{ GeV}^2/c^4$. For $\mathcal{M}_{\nu}^2 < -4.5 \text{ GeV}^2/c^4$, where just continuum and combinatorial backgrounds are present, we assume that $f_{B^-}^{\pm} = 0$, and we compute $f_{qq}^{\pm} = 1 - f_{B\bar{B}}^{\pm}$.

sample of events with dilution \mathcal{D} , reads

$$\frac{\mathcal{N}_{mix}}{\mathcal{N}_{mix} + \mathcal{N}_{unmix}} = \chi_d \cdot \mathcal{D} + \frac{1 - \mathcal{D}}{2}, \quad (2)$$

where, neglecting the difference $\Delta\Gamma_d$ between the two mass eigenstates, the integrated mixing rate χ_d is related to the product $x = \Delta m_d \cdot \tau_{B^0}$ by the relation

$$\chi_d = \frac{x^2}{2(1 + x^2)}. \quad (3)$$

We describe the Δt distribution as the sum of the decay probabilities for signal and background events:

$$\begin{aligned}
\mathcal{F}^\pm(\Delta t, \sigma_{\Delta t}, \mathcal{M}_\nu^2 | \tau_{B^0}, \Delta m_d) &= f_{q\bar{q}}^\pm(\mathcal{M}_\nu^2) \cdot \mathcal{F}_{q\bar{q}}^\pm(\Delta t, \sigma_{\Delta t}) \\
&+ f_{B\bar{B}}^\pm(\mathcal{M}_\nu^2) \cdot \mathcal{F}_{B\bar{B}}^\pm(\Delta t, \sigma_{\Delta t}) \\
&+ \mathcal{S}_{B^-} f_{B^-}^\pm(\mathcal{M}_\nu^2) \cdot \mathcal{F}_{B^-}^\pm(\Delta t, \sigma_{\Delta t}) \\
&+ [1 - \mathcal{S}_{B^-} f_{B^-}^\pm(\mathcal{M}_\nu^2) - f_{B\bar{B}}^\pm(\mathcal{M}_\nu^2) - f_{q\bar{q}}^\pm(\mathcal{M}_\nu^2)] \\
&\cdot \mathcal{F}_{\bar{B}^0}^\pm(\Delta t, \sigma_{\Delta t} | \tau_{B^0}, \Delta m_d),
\end{aligned} \tag{4}$$

where the functions \mathcal{F}_i^\pm represent the probability density functions (PDF) for signal ($i = \bar{B}^0$), peaking B^- ($i = B^-$), $B\bar{B}$ combinatorial ($i = B\bar{B}$), and continuum ($i = q\bar{q}$) events, and the superscript $+(-)$ applies to unmixed (mixed) events. To account for the $\pm 50\%$ uncertainty on the isospin assumption (see Section 3.3), we introduce in the PDF a global scale factor \mathcal{S}_{B^-} multiplying the fractions $f_{B^-}^\pm$, equal for mixed and unmixed events, which we float in the fit but constrained to unity with 0.5 error.

The signal PDF is obtained from Eq. 1 modified to account for the finite resolution of the detector. The resolution function is expressed as the sum of three Gaussian functions, defined as “narrow”, “wide” and “outlier”:

$$\mathcal{R}(\delta\Delta t, \sigma_{\Delta t}) = \frac{(1 - f_w - f_o)}{\sqrt{2\pi} S_n \sigma_{\Delta t}} e^{-\frac{(\delta\Delta t - o_n)^2}{2S_n^2 \sigma_{\Delta t}^2}} + \frac{f_w}{\sqrt{2\pi} S_w \sigma_{\Delta t}} e^{-\frac{(\delta\Delta t - o_w)^2}{2S_w^2 \sigma_{\Delta t}^2}} + \frac{f_o}{\sqrt{2\pi} S_o} e^{-\frac{(\delta\Delta t - o_o)^2}{2S_o^2}}, \tag{5}$$

where $\delta\Delta t$ is the difference between the measured and the true value of Δt , o_n and o_w are offsets, the factors S_n and S_w account for possible misestimation of $\sigma_{\Delta t}$. The outlier term, described by a Gaussian function of fixed width S_o and offset o_o , is introduced to describe events with badly measured Δt , and accounts for less than 1% of the events.

We divide signal events according to the origin of the tag lepton into primary, cascade, and decay-side tags. A primary tag is produced in the direct decay $B^0 \rightarrow \ell^+ \nu_\ell X$. These events are described by Eq. 1, with \mathcal{D} close to one (a small deviation from unity is expected due to hadron misidentification, leptons from J/ψ , etc.). We expect small values of o_n and o_w for primary tags, because the lepton originates from the B^0 decay point.

Cascade tags, produced in the process $B^0 \rightarrow DX, D \rightarrow \ell Y$, are suppressed by the cut on the lepton momentum but still exist at a level of 9% as we obtain by floating their relative abundance as an additional parameter in the Δm_d fit on data. The lepton production point is displaced from the B^0 decay point due to the finite lifetime of charm mesons and the e^+e^- energy asymmetry. This results in a significant positive value of the offsets for this category. Compared with the primary tag, the cascade lepton usually has the opposite charge correlation with the B^0 flavor. The same charge correlation is obtained when the charm meson is produced from the hadronization of the virtual W from B^0 decay, usually referred to as “Upper Vertex”, which results in the production of two opposite-flavor charm mesons. We account for these facts by applying Eq. 1 to the cascade tag events with negative dilution $\mathcal{D}_{C\ell} = -(1 - 2f_{UV}) = -0.65 \pm 0.08$, where we take from the PDG [11] the ratio of the inclusive semileptonic branching ratios of the b quark $f_{UV} = \frac{BR(\bar{b} \rightarrow c \rightarrow \ell^+)}{BR(\bar{b} \rightarrow c \rightarrow \ell^+) + BR(\bar{b} \rightarrow \bar{c} \rightarrow \ell^-)} = 0.17 \pm 0.04$ (the contribution to the dilution from other sources associated with the $\pi_s^+ \ell$ candidate, such as fake hadrons, is negligible).

Decay-side tags are produced by the semileptonic decay of the unreconstructed D^0 . Therefore they do not carry any information about τ_{B^0} or Δm_d . The PDF for both mixed and unmixed

contributions is a purely exponential function, with an effective lifetime representing the displacement of the lepton production point from the \bar{B}^0 decay point due to the finite lifetime of the D^0 . We determine the fraction of these events by fitting the $\cos\theta_{\pi_s^+\ell}$ distribution (see Fig. 4), where $\theta_{\pi_s^+\ell}$ is the angle between the soft pion and the tag lepton. Using the results of the $\cos\theta_{\pi_s^+\ell}$ fit we parameterize the probability for each event to have a decay-side tag as a third order polynomial function of $\cos\theta_{\pi_s^+\ell}$ (see Fig. 4).

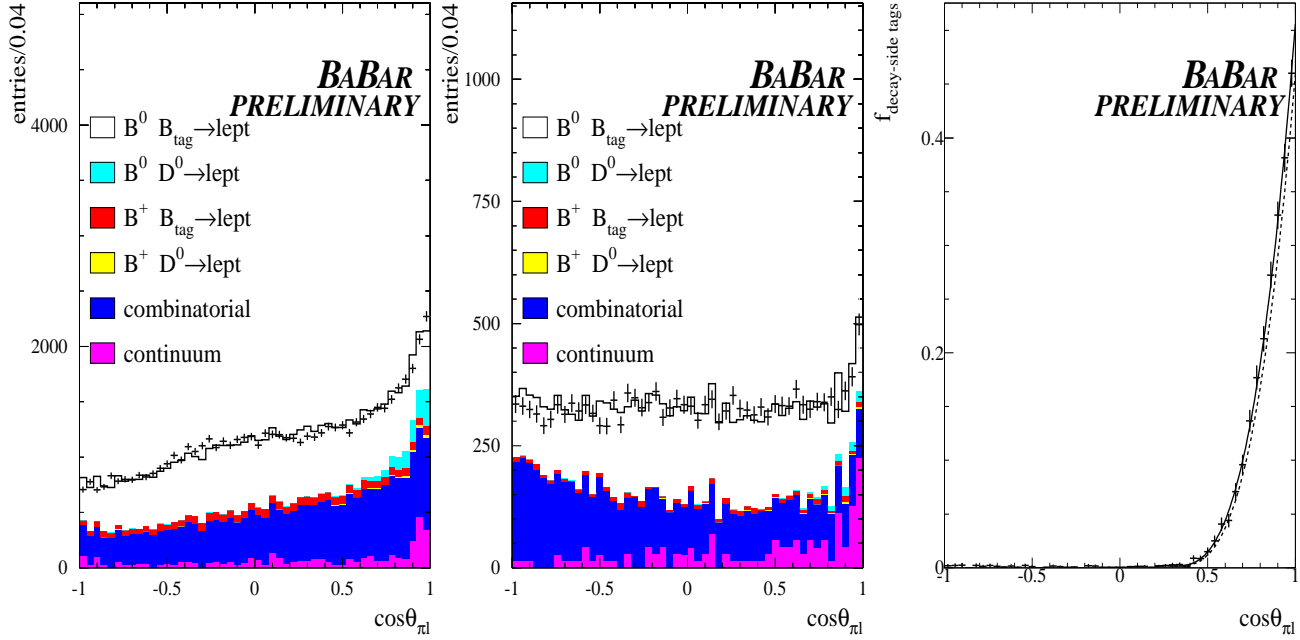


Figure 4: Distribution of $\cos\theta_{\pi_s^+\ell}$ for unmixed (left) and mixed (center) events. The points with error bars are the data, the shaded histograms show the various sample components after the fit. Right plot shows the fraction of tags from D^0 decay as a function of $\cos\theta_{\pi_s^+\ell}$ for signal events. The points with error bars are the data, the solid line is the resulting fitted function and the dashed line is the simulation prediction.

The signal PDF for both mixed and unmixed events consists of the sum of primary, cascade, and decay-side tags, each convoluted with its own resolution function. The parameters S_n , S_w , S_o , f_w , and f_o are common to the three terms, while each tag type has different offsets (o_n , o_w). To reduce the systematic error, some other parameters, in addition to τ_{B^0} and Δm_d are free in the fit, namely, all the parameters of the resolution functions, the dilution of the primary tags, the fraction of cascade tags, and the effective lifetime of the decay-side tags. We fix the other parameters (dilution of cascade tags, fraction of decay-side tags) to their values, obtained as described above, and then vary them within their error ranges to assess the corresponding systematic error, as we have described above.

We adopt a similar PDF for peaking B^- background, accounting for primary, cascade, and decay terms. Because B^- mesons do not oscillate, we use a pure exponential PDF for the primary and cascade tags with lifetime $\tau_{B^-} = 1.671 \pm 0.018$ ps [12]. We force the parameters of the resolution function to equal those for the corresponding signal term.

We describe continuum events with an exponential function convoluted with a three-Gaussian resolution function. The mixed and unmixed terms have separate effective lifetime parameters. All the parameters of the continuum resolution function are set equal to those of the signal, except for the offsets, which are free in the fit.

The PDF for combinatorial $B\bar{B}$ background accounts for oscillating and non-oscillating terms. It has the same functional form as the PDF for peaking events, but with independent parameters for the oscillation frequency and the lifetimes, which we interpret as effective parameters that do not necessarily have a precise physical interpretation. The parameters S_n , S_w , and f_w are set to the same values as those in the signal.

4 RESULTS

We first perform the measurement on several Monte Carlo samples. We validate each term of the PDF by first fitting signal events, for primary, cascade and decay-side tags separately, and then adding them together. We then add peaking B^- background, and finally add the $B\bar{B}$ combinatorial background. We observe the following features:

- The event selection introduces a bias of $(+0.016 \pm 0.005)$ ps on τ_{B^0} and $(+0.0027 \pm 0.0014)$ ps⁻¹ on Δm_d .
- The boost approximation introduces a sizable bias on Δm_d (-0.0066 ps⁻¹), as observed by fitting the true Δz distribution. This bias disappears however when we fit the smeared Δz and allow for the experimental resolution in the fit function.
- Introducing B^- peaking background does not introduce any additional bias.
- Adding combinatorial $B\bar{B}$ events, we introduce an additional bias of $+0.011$ ps on τ_{B^0} and of -0.0058 ps⁻¹ on Δm_d .
- All the parameters with a clear physical meaning are consistent with their expected value; in particular the isospin scale factor $\mathcal{S}_{B^-} = 1.04 \pm 0.06$ is consistent with unity.

Based on these observations, we correct the data results by subtracting 0.027 ps from τ_{B^0} , and adding 0.0031 ps⁻¹ to Δm_d . We assign 100% of the correction as a systematic uncertainty due to the observed biases.

Although we determine the parameters for continuum events directly from the fit to on-peak data, we independently fit the off-peak events to verify the consistency with the on-peak continuum results.

We finally perform the fit to the on-peak data. Together with Δm_d and τ_{B^0} , we float most of the parameters describing the peaking B^- , $B\bar{B}$ combinatorial, and continuum background events. The values of Δm_d and τ_{B^0} were blinded until completion of the study of the systematic errors. The unblinded fit results are $\tau_{B^0} = (1.5280 \pm 0.0084$ (stat.)) ps, and $\Delta m_d = (0.5200 \pm 0.0043$ (stat.)) ps⁻¹. We correct these values for the biases measured in the Monte Carlo simulation, obtaining the preliminary *BABAR* results

$$\begin{aligned} \tau_{B^0} &= (1.501 \pm 0.008 \text{ (stat.)} \pm 0.030 \text{ (syst.)}) \text{ ps,} \\ \Delta m_d &= (0.523 \pm 0.004 \text{ (stat.)} \pm 0.007 \text{ (syst.)}) \text{ ps}^{-1}. \end{aligned} \tag{6}$$

The correlation between Δm_d and τ_{B^0} is -1.2% . Δm_d has sizable correlations with \mathcal{S}_{B^-} (7.7%) and S_o (7.4%). τ_{B^0} is correlated with f_o (13%) and with a parameter corresponding to the fraction of mixed combinatorial B^- events (20%). The complete set of fit parameters is reported in Table 1.

Details on the systematic error are reported in Section 5. Figure 5 shows the comparison between the data and the fit function projected on Δt , for a sample of events enriched in signal by the cut $\mathcal{M}_\nu^2 > -2.5 \text{ GeV}^2/c^4$; Fig. 6 shows the same comparison for events in the background region. Figure 7 shows the plot of the time-dependent asymmetry $\mathcal{A}(\Delta t) = \frac{N_{Unmixed}(\Delta t) - N_{Mixed}(\Delta t)}{N_{Unmixed}(\Delta t) + N_{Mixed}(\Delta t)}$ for events in the signal region and events in the background region.

The agreement between the fitting function and the data distribution is good both in the signal and in the background regions. We perform a set of parametrized Monte Carlo experiments to assess the quality of the fit. The probability to obtain a lower likelihood is 50% .

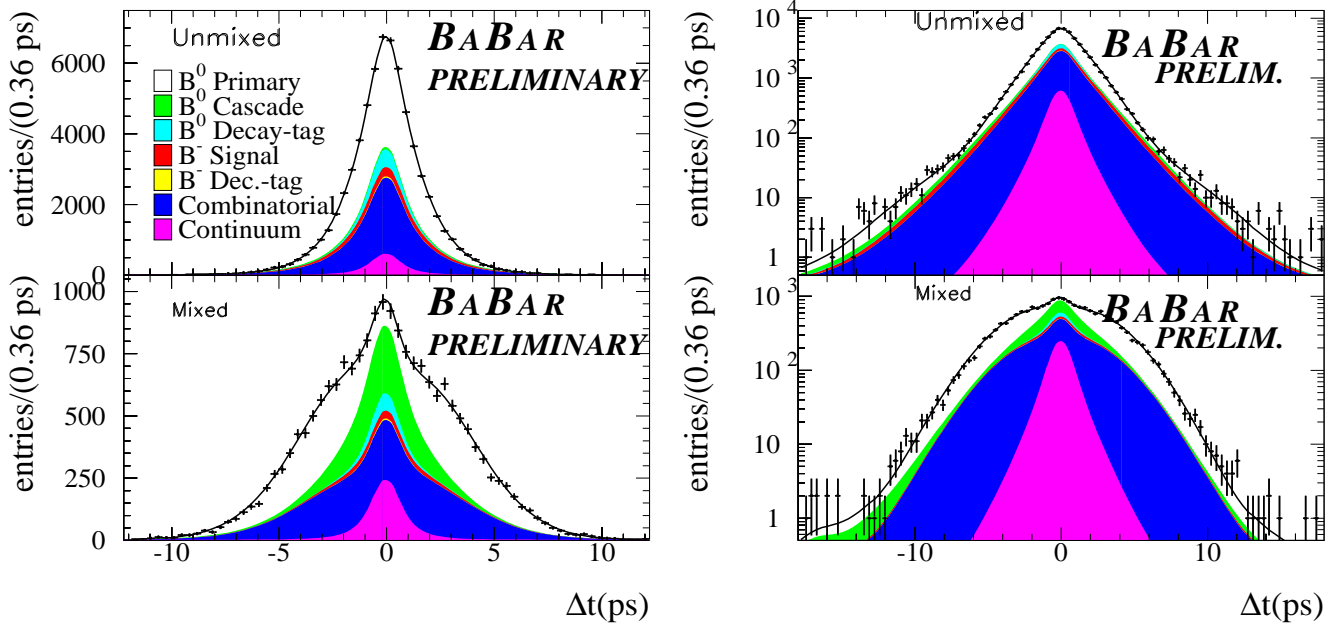


Figure 5: Distribution of Δt for unmixed (top) and mixed (bottom) events in the signal \mathcal{M}_ν^2 region with linear (left) and logarithmic (right) scales. The points show the data, the curve is the projection of the fit result, and the shaded areas from bottom to top are the contributions from continuum, $B\bar{B}$ combinatorial, peaking B^- with decay-side tag, peaking B^- with primary tag, signal with decay-side tag, signal with cascade tag, and signal with primary tag.

5 SYSTEMATIC UNCERTAINTIES

The systematic errors are summarized in Table 2. We consider the following sources of systematic uncertainty:

1. Sample composition: the fraction of peaking B^- events in the sample, \mathcal{S}_{B^-} , is free in the fit; therefore we do not assign any systematic error on this fraction. As mentioned in Section 3.3,

Table 1: Parameters used in the PDFs from which the likelihood is calculated. The second column shows how they are treated in the fit. The third (fourth) column gives the value employed in the data (MC) for the parameters that are fixed or used as a constraint. The last column shows the sample in which the parameter is used. The first set of parameters corresponds to peaking events, the second to $B\bar{B}$ combinatorial events, and the third to continuum parameters. The last set refers to those parameters of the resolution function that are common to all the data sets. $\mathcal{P}\ell$, $\mathcal{C}\ell$ and $\mathcal{D}\ell$ refer to primary, cascade and decay-side tags, respectively. The symbols o , S , and f correspond to offsets, scale factors and fractions in the resolution function; the symbols α and ρ correspond to the fraction of decay-side tags and the fraction of mixed events in the decay-side tag sample, respectively.

| Parameter | Usage | data | M.C. | Sample |
|---|---------------------------------|----------------------|--------------------|--|
| τ_{B^0} (ps) | free | 1.501 ± 0.008 | 1.575 ± 0.006 | $\bar{B}^0 \mathcal{P}\ell, \mathcal{C}\ell$ |
| Δm_d (ps $^{-1}$) | free | 0.523 ± 0.004 | 0.469 ± 0.002 | $\bar{B}^0 \mathcal{P}\ell, \mathcal{C}\ell$ |
| τ_{D_e} (ps) | free | 0.16 ± 0.02 | 0.22 ± 0.01 | \bar{B}^0, B^- and unmixed- $B\bar{B}, \mathcal{D}\ell$ |
| τ_{B^-} (ps) | fixed | 1.671 ± 0.018 | 1.65 (M.C.) | B^- and $B\bar{B}$ |
| f_{B^-} | constrained (1.0 ± 0.5) | 1.11 ± 0.11 | 1.04 ± 0.06 | |
| $f_{\mathcal{C}\ell}$ | free | 0.095 ± 0.003 | 0.077 ± 0.002 | \bar{B}^0 |
| $D_{\mathcal{P}\ell}$ | free | 0.998 ± 0.002 | 0.969 ± 0.002 | $\bar{B}^0, \mathcal{P}\ell$ |
| $D_{\mathcal{C}\ell}$ | fixed | 0.65 ± 0.08 | 0.536 | $\bar{B}^0, \mathcal{C}\ell$ |
| $o_{\mathcal{P}\ell, N}(= o_{\mathcal{P}\ell, W})$ (ps) | free | -0.012 ± 0.008 | -0.012 ± 0.004 | $\bar{B}^0, B^- \mathcal{P}\ell$ |
| $o_{\mathcal{C}\ell, N}$ (ps) | free | -0.17 ± 0.06 | -0.52 ± 0.04 | $\bar{B}^0 \mathcal{C}\ell$ |
| $o_{\mathcal{C}\ell, W}$ (ps) | free | -6.2 ± 0.8 | -5.8 ± 0.5 | $\bar{B}^0 \mathcal{C}\ell$ |
| $o_{\mathcal{D}\ell, N}(= o_{\mathcal{D}\ell, W})$ (ps) | free | -0.13 ± 0.02 | -0.13 ± 0.01 | $\bar{B}^0, B^-, \mathcal{D}\ell$ |
| S_O (ps) | free | 24.7 ± 3.6 | 41.6 ± 0.3 | \bar{B}^0, B^- and $\mathcal{D}\ell$ |
| f_O | free | 0.00004 ± 0.00013 | 0.0013 ± 0.0004 | \bar{B}^0, B^- and $\mathcal{D}\ell$ |
| $\tau_{B^0}^{BKG}$ (ps) | free | 1.24 ± 0.04 | 1.26 ± 0.07 | $B\bar{B}$ |
| Δm_d^{BKG} (ps $^{-1}$) | free | 0.45 ± 0.01 | 0.50 ± 0.02 | $B\bar{B}$ |
| $\tau_{D_e^{mixed}}^{BKG}$ (ps) | free | 2.4 ± 0.5 | 1.2 ± 1.7 | $B\bar{B}, \mathcal{D}\ell$ (mixed only) |
| f^{B^-} | free | 0.63 ± 0.01 | 0.60 ± 0.02 | $B\bar{B}$ |
| g^{B^-} | free | 0.043 ± 0.001 | 0.078 ± 0.003 | $B\bar{B}$ |
| f_{bcl}^{BKG} | free | 0.0001 ± 0.0001 | 0.01 ± 0.01 | $B\bar{B}$ |
| $D_{\mathcal{P}\ell}^{BKG}$ | free | 0.997 ± 0.003 | 0.986 ± 0.004 | $B\bar{B}$ (\bar{B}^0 only) |
| $o_{BKG, \mathcal{P}\ell}$ (ps) | free | -0.06 ± 0.03 | -0.07 ± 0.12 | $B\bar{B}$ |
| $o_{BKG, \mathcal{C}\ell}$ (ps) | free | -16.7 ± 2.1 | -1.8 ± 0.4 | $B\bar{B}$ |
| $o_{BKG, \mathcal{D}\ell}$ (ps) | free | 0.01 ± 0.02 | -0.06 ± 0.01 | $B\bar{B}, \mathcal{D}\ell$ |
| $\alpha_{B^0}^{BKG}$ | free | 0.28 ± 0.02 | 0.29 ± 0.04 | $B\bar{B}$ (\bar{B}^0 only) |
| $\rho_{B^0}^{BKG}$ | free | 0.0 ± 0.1 | 0.2 ± 0.1 | $B\bar{B}$ (\bar{B}^0 only) |
| $\alpha_{B^+}^{BKG}$ | free | 0.039 ± 0.004 | 0.134 ± 0.006 | $B\bar{B}$ (B^- only) |
| $\rho_{B^+}^{BKG}$ | free | 0.03 ± 0.11 | 0.2 ± 0.1 | $B\bar{B}$ (B^- only) |
| S_O^{BKG} (ps) | free | 40.2 ± 0.3 | 48 ± 1 | $B\bar{B}$ |
| f_O^{BKG} | free | 0.0046 ± 0.0014 | 0.0011 ± 0.0007 | $B\bar{B}$ |
| τ_{lq} (ps) | free | 0.17 ± 0.02 | - | Continuum |
| $o_{lq, N} = o_{lq, W}$ (ps) | free | -0.05 ± 0.01 | - | Continuum |
| S_N | free | 0.997 ± 0.006 | 0.996 ± 0.004 | common to all |
| S_W | free | 3.74 ± 0.14 | 2.48 ± 0.06 | common to all |
| f_W | free | 0.024 ± 0.001 | 0.036 ± 0.002 | common to all |
| o_O (ps) | fixed | 0_{18} | 0 | common to all |
| $\rho(\tau_{B^0}, \Delta m_d)$ | | -0.012 | -0.081 | |

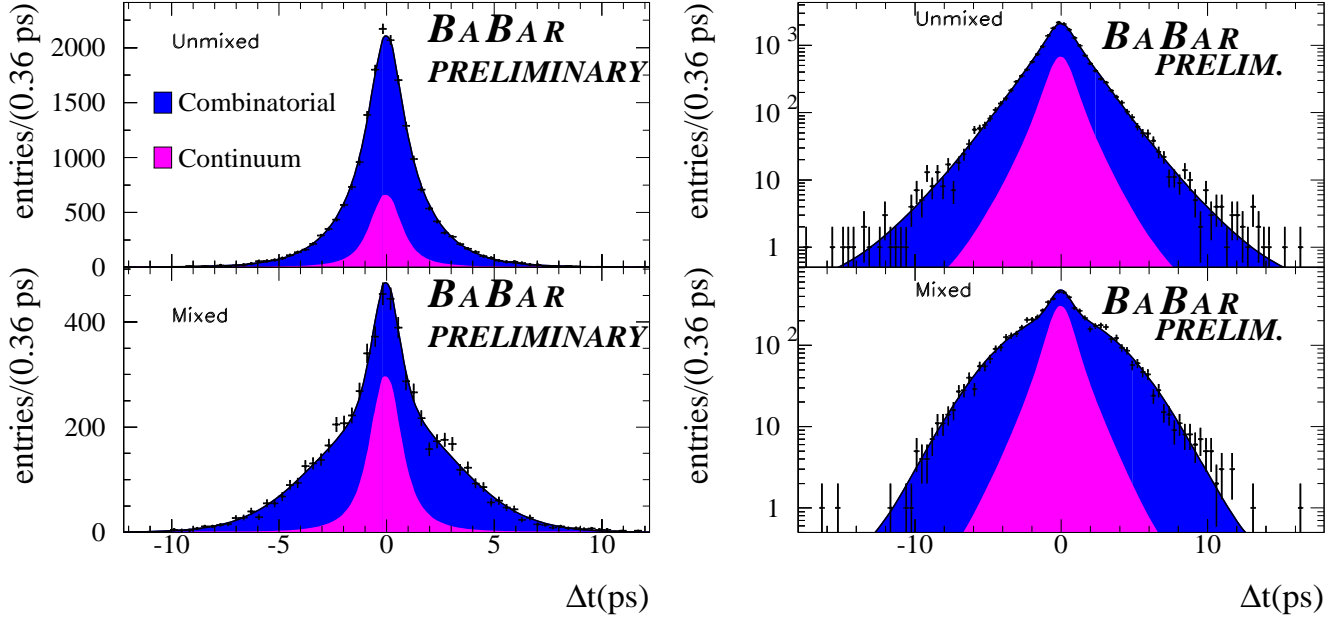


Figure 6: Distribution of Δt for unmixed (top) and mixed (bottom) events in the background \mathcal{M}_B^2 region with linear (left) and logarithmic (right) scales. The points show the data, the curve is the projection of the fit result, and the shaded areas are the contributions from continuum and $B\bar{B}$ combinatorial background.

there is a $\pm 2.3\%$ systematic uncertainty on the background rate due to possibly peaking combinatorial background. We therefore vary the fraction of $B\bar{B}$ events in the signal region by that amount, repeat the fit, and add the variation in the result to the systematic error (entry (a) of Table 2). We neglect the statistical error on the sample composition because it is significantly smaller than this systematic effect.

2. Analysis bias (entry b): we take 100% of the bias observed in the fit on the Monte Carlo sample.
3. Signal and background PDF description: most of the parameters in the PDF are free in the fit and therefore do not contribute to the systematic error. We vary the parameters that are fixed in the fit by their uncertainty, repeat the fit, and take the corresponding variation in τ_{B^0} and Δm_d as systematic errors. We take the uncertainty on τ_{B^-} (entry (c)), and on $D_{C\ell}$ (entry (d)) from the PDG [11].
4. We consider effects due to the detector z scale (entry (e)), the knowledge of the PEP-II boost (entry (f)), the actual position of the beam spot (entry (g)), and SVT alignment (entry (h)). Detailed studies of these effects have been performed in *BABAR* in other mixing and lifetime analyses (dilepton [13] and fully reconstructed $\bar{B}^0 \rightarrow D^{*+}\ell^-\bar{\nu}_\ell$ [14] analyses) and provided consistent results. As the methods for vertex reconstruction are very similar we provisionally take our systematic error due to these effects from Ref. [14].

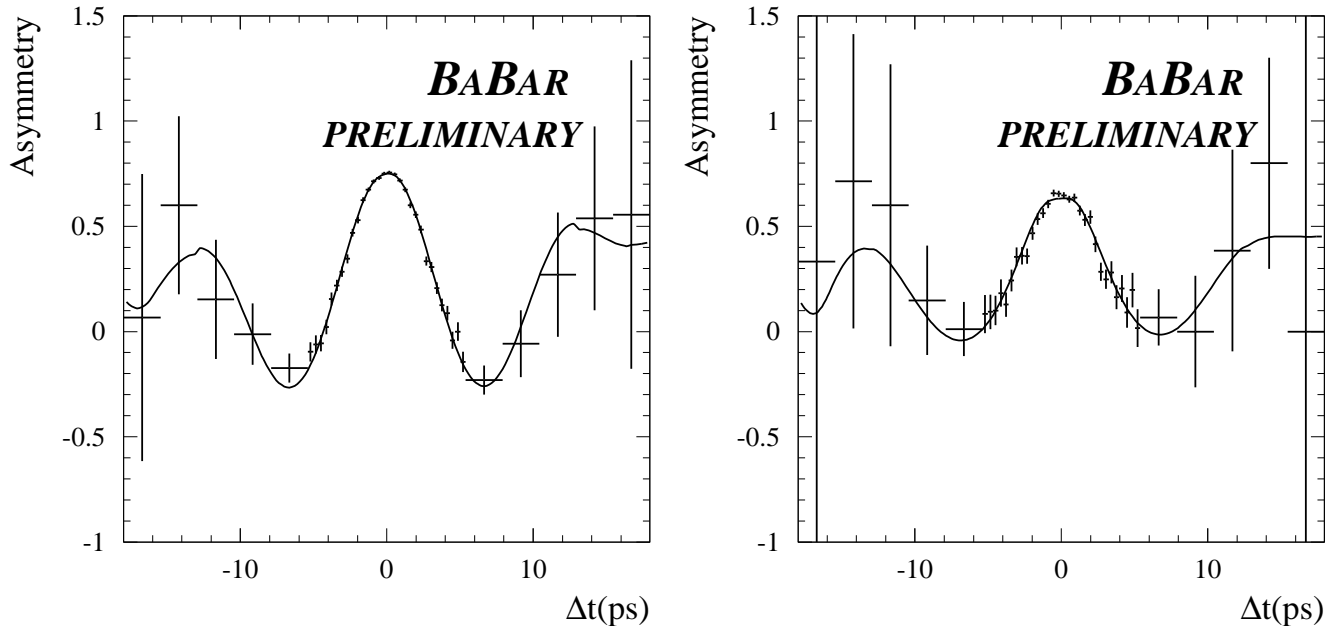


Figure 7: Asymmetry between unmixed and mixed events as a function of Δt , for events in the signal region (left) and in the background region (right). Points with error bars are the data, and the curve is a projection of the fit result.

5. We vary the parameters describing the fraction of decay-side tags by their statistical errors (entry (i)).
6. Binned fitting: we vary the number of bins in Δt from 100 to 250 and in $\sigma_{\Delta t}$ from 20 to 50, and we repeat the fit. Alternatively, we use the average value of the likelihood in the bin instead of the value corresponding to the center of the bin. We take the systematic error to be the maximum variation with reference to the default result (entry (j)).
7. Outlier description: we vary the value of the offset of the outlier Gaussian from -5 ps to 5 ps. Alternatively, we use a flat PDF for their description (entry (k)).
8. Fit range: we vary the Δt fit range from ± 18 ps to ± 10 ps and the $\sigma_{\Delta t}$ range between 1.8 ps and 4.2 ps (entry (l)).

6 CONSISTENCY CHECKS

We rely on the assumption that the parameters of the background PDF do not depend on \mathcal{M}_v^2 . We verify this assumption for the continuum background with the fit to the off-peak events. To check this assumption for the $B\bar{B}$ combinatorial PDF, we perform several cross checks on the data and the Monte Carlo. We compare the simulated $B\bar{B}$ Δt distribution in several independent regions of \mathcal{M}_v^2 with Kolmogorov-Smirnov tests and always obtain a reasonable probability for agreement. We fit $B\bar{B}$ events separately in the signal and background \mathcal{M}_v^2 region and compare the parameters of

Table 2: Systematic uncertainties.

| Source | Variation | $\delta\tau_{B^0}$ (ps) | $\delta\Delta m_d$ (ps^{-1}) |
|--|----------------------|-------------------------|---|
| (a) $B\bar{B}$ fraction | $\pm 2.3\%$ | ± 0.001 | ± 0.001 |
| (b) Analysis bias | - | ± 0.027 | ± 0.003 |
| (c) τ_{B^-} | 1.671 ± 0.018 ps | ± 0.002 | ± 0.001 |
| (d) $\mathcal{D}_{\mathcal{C}\ell}$ | 0.65 ± 0.08 | ± 0.005 | ± 0.001 |
| (e) z scale | - | ± 0.006 | ± 0.002 |
| (f) PEP-II boost | - | ± 0.002 | ± 0.001 |
| (g) Alignment | - | ± 0.006 | ± 0.003 |
| (h) Beam spot position | - | ± 0.005 | ± 0.001 |
| (i) Decay-side tags | - | ± 0.002 | ± 0.001 |
| (j) Binning | - | ± 0.002 | ± 0.002 |
| (k) Outlier | - | ± 0.001 | ± 0.002 |
| (l) Δt and $\sigma_{\Delta t}$ cut | - | ± 0.008 | ± 0.003 |
| Total | | ± 0.030 | ± 0.007 |

the PDF. We fit the signal plus background Monte Carlo events in the signal region only, fixing all the parameters of the $B\bar{B}$ sample to the values obtained in a fit in the background region, and do not see any appreciable deviation from the result of the full fit. Finally, we repeat the fit both on the data and the Monte Carlo using different \mathcal{M}_v^2 ranges for the background region. Once again, we do not observe any appreciable difference in τ_{B^0} and Δm_d relative to the default result.

7 CONCLUSION

We have performed a measurement of Δm_d and τ_{B^0} on a sample of 50000 partially reconstructed, lepton-tagged $\bar{B}^0 \rightarrow D^{*+} \ell^- \bar{\nu}_\ell$ decays. We obtain the following preliminary results:

$$\begin{aligned}\tau_{B^0} &= (1.501 \pm 0.008 \text{ (stat.)} \pm 0.030 \text{ (syst.)}) \text{ ps,} \\ \Delta m_d &= (0.523 \pm 0.004 \text{ (stat.)} \pm 0.007 \text{ (syst.)}) \text{ ps}^{-1}.\end{aligned}$$

These preliminary values are consistent with published measurements of τ_{B^0} and Δm_d performed by *BABAR* with different data sets, and with the world averages computed by the Heavy Flavor Averaging Group [12], as can be seen in table 3. The error we obtain on Δm_d is comparable to the uncertainty on the present world average.

8 ACKNOWLEDGMENTS

We are grateful for the extraordinary contributions of our PEP-II colleagues in achieving the excellent luminosity and machine conditions that have made this work possible. The success of this project also relies critically on the expertise and dedication of the computing organizations that support *BABAR*. The collaborating institutions wish to thank SLAC for its support and the kind hospitality extended to them. This work is supported by the US Department of Energy and National Science Foundation, the Natural Sciences and Engineering Research Council (Canada),

Table 3: Comparison of this result with previous *BABAR* measurements and with the world average. In the case of the world average, we report the total error; in all other cases we show the statistical and systematic errors separately. P.R. means partial reconstruction.

| Method | Δm_d (ps) $^{-1}$ | τ_{B^0} (ps) | Reference |
|--|-----------------------------|-----------------------------|-----------|
| <i>BABAR</i> Hadronic | $0.516 \pm 0.016 \pm 0.010$ | $1.546 \pm 0.032 \pm 0.022$ | [15, 16] |
| <i>BABAR</i> $\ell\ell$ | $0.493 \pm 0.012 \pm 0.009$ | – | [13] |
| <i>BABAR</i> $D^{*-}\ell^+\nu_\ell$ | $0.492 \pm 0.018 \pm 0.013$ | $1.523 \pm 0.024 \pm 0.022$ | [14] |
| <i>BABAR</i> $D^{*-}\ell^+\nu_\ell$ (P.R.) | – | $1.529 \pm 0.012 \pm 0.029$ | [3] |
| <i>BABAR</i> $D^{*-}\pi^+$ (P.R.) | – | $1.533 \pm 0.034 \pm 0.038$ | [4] |
| World Average | 0.502 ± 0.007 | 1.536 ± 0.014 | [12] |
| This Measurement | $0.523 \pm 0.004 \pm 0.007$ | $1.501 \pm 0.008 \pm 0.030$ | |

Institute of High Energy Physics (China), the Commissariat à l’Energie Atomique and Institut National de Physique Nucléaire et de Physique des Particules (France), the Bundesministerium für Bildung und Forschung and Deutsche Forschungsgemeinschaft (Germany), the Istituto Nazionale di Fisica Nucleare (Italy), the Foundation for Fundamental Research on Matter (The Netherlands), the Research Council of Norway, the Ministry of Science and Technology of the Russian Federation, and the Particle Physics and Astronomy Research Council (United Kingdom). Individuals have received support from CONACyT (Mexico), the A. P. Sloan Foundation, the Research Corporation, and the Alexander von Humboldt Foundation.

References

- [1] *BABAR* Collaboration, B. Aubert *et al.*, Nucl. Instrum. Methods A **479**, 1 (2002).
- [2] G.C. Fox and S. Wolfram, Phys. Rev. Lett. **41**, 1581 (1978).
- [3] *BABAR* Collaboration, B. Aubert *et al.*, Phys. Rev. Lett. **89**, 011802 (2002).
- [4] *BABAR* Collaboration, B. Aubert *et al.*, Phys. Rev. D **67**, 091101 (2003).
- [5] *BABAR* Collaboration, B. Aubert *et al.*, Phys. Rev. Lett. **92**, 251802 (2004).
- [6] ARGUS Collaboration, H. Albrecht *et al.*, Phys. Lett. B **324**, 249 (1994).
- [7] CLEO Collaboration, J. Bartelt *et al.*, Phys. Rev. Lett. **71**, 1680 (1993).
- [8] DELPHI Collaboration, P. Abreu *et al.*, Phys. Lett. B **510**, 55 (2001).
- [9] OPAL Collaboration, G. Abbiendi *et al.*, Phys. Lett. B **482**, 15 (2000).
- [10] CLEO Collaboration, M. Artuso *et al.*, Phys. Rev. Lett. **80**, 3193 (1998).
- [11] Particle Data Group, S. Eidelman *et al.*, Phys. Lett. B **592**, 1 (2004).
- [12] Heavy Flavor Averaging Group: <http://www.slac.stanford.edu/xorg/hfag/>

- [13] *BABAR* Collaboration, B. Aubert *et al.*, Phys. Rev. Lett. **88**, 221803 (2002).
- [14] *BABAR* Collaboration, B. Aubert *et al.*, Phys. Rev. D **67**, 072002 (2003).
- [15] *BABAR* Collaboration, B. Aubert *et al.*, Phys. Rev. Lett. **87**, 201803 (2001).
- [16] *BABAR* Collaboration, B. Aubert *et al.*, Phys. Rev. Lett. **88**, 221802 (2002).